Multiscale modeling of electrical conductivity of R-BAPB polyimide plus carbon nanotubes nanocomposites

S. V. Larin and S. V. Lyulin
Institute of Macromolecular Compounds, Russian Academy of Sciences, V.O. Bol'shoi pr. 31, 199004 St. Petersburg, Russian Federation

P. A. Likhomanova*
National Research Center "Kurchatov Institute," 123182, Moscow, Russia

K. Yu. Khromov†
National Research Center "Kurchatov Institute," 123182, Moscow, Russia and Moscow Institute of Physics and Technology (State University), 117303, Moscow, Russia

A. A. Knizhnik and B. V. Potapkin
Kintech Laboratory Ltd., 123182, Moscow, Russia and National Research Center "Kurchatov Institute," 123182, Moscow, Russia

(Received 20 May 2020; revised 31 March 2021; accepted 25 May 2021; published 22 June 2021)

The electrical conductivity of the polyimide R-BAPB polymer filled with single-wall carbon nanotubes (CNT) is modeled using a multiscale approach. The modeling starts with molecular dynamics simulations of time-dependent atomic configurations of polymer-filled CNTs junctions. Then the atomic positions obtained in the first step are used to perform fully first-principles microscopic calculations of the CNTs junctions contact resistances using the quantum transport technique based on Green's functions. Finally, those contact resistances are supplied as an input to a statistical calculation of a CNTs ensemble conductivity using a Monte Carlo percolation model. We discuss the effects of various geometrical peculiarities of CNTs mutual orientation, including an angle φ between nanotubes axes, a CNTs overlap, a separation between CNTs, as well as CNTs sizes, chiralities, CNTs functionalization on the contact resistance of CNTs junctions. The results of the first-principles calculations show that of all the considered geometrical peculiarities the angle dependence of CNTs intersections has the most significant influence on contact resistance of polymer-filled CNTs junctions. A simple fitting model, describing the dependence of a junction conductance of that angle, is proposed. Incorporating into the percolation model this strong dependence as well as CNTs agglomeration pushed the calculated values of electrical conductivity of the composite just above the percolation threshold below 0.01 S/m, which is within the experimental range for composites with various base polymers. Possible mechanisms for further reduction of composites conductivity are discussed.

DOI: 10.1103/PhysRevMaterials.5.066002

I. INTRODUCTION

Polymer materials, while possessing some unique and attractive qualities, such as low weight, high strength, resistance to chemicals, and ease of processing, are for the most part insulators. If methods could be devised to turn common insulating polymers into conductors, that would open great prospects for using such materials in many more areas than they are currently used. These areas may include organic solar cells, printing electronic circuits, light-emitting diodes, actuators, supercapacitors, chemical sensors, and biosensors [1].

Since the reliable methods for carbon nanotubes (CNT) fabrication had been developed in the 1990s, growing attention has been paid to the possibility of dispersing CNTs in polymers, where CNTs junctions may form a percolation network and turn an insulating polymer into a good conductor when a percolation threshold is overcome. An additional benefit of using such polymer/CNTs nanocomposites instead of intrinsically conducting polymers, such as polyaniline [2] for example, is that dispersed CNTs, besides providing electrical conductivity, enhance polymer mechanical properties as well.

CNTs enhanced polymer nanocomposites have been intensively investigated experimentally, including composites conductivity [3]. As for the theoretical research in this area, the results are more modest. If one is concerned with nanocomposite conductivity, its value depends on many factors, among which are the polymer type, CNTs density, nanocomposite preparation technique, CNTs and their junctions geometry, a possible presence of defects in CNTs, and others. Taking all these factors into account and obtaining quantitatively correct results in modeling is a very challenging task since the resulting conductivity is formed at different length scales: At the microscopic level it is influenced by

*likhomanovapa@gmail.com
†khromov_ky@nrcki.ru

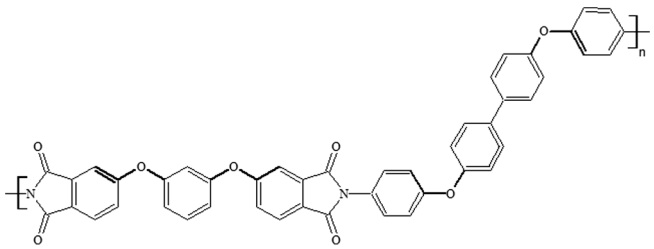

FIG. 1. The chemical structure of R-BAPB polyimide. The thick bonds correspond to the dihedral angles used to estimate the local relaxation properties of the polyimide chains.

the CNTs junctions contact resistance and at the mesoscopic level it is determined by percolation through a network of CNTs junctions. Thus a consistent multiscale method for the modeling of conductivity, starting from atomistic first-principles calculations of electron transport through CNTs junctions, is necessary.

Due to the complexity of this multiscale task, the majority of investigations in the area are carried out in some simplified forms; this is especially true for the underlying part of the modeling: determination of CNTs junction contact resistance. For the contact resistance either experimental values as in Ref. [4] or the results of phenomenological Simmons model as in Refs. [5–8] are usually taken, or even an arbitrary value of contact resistance reasonable by an order of magnitude may be set [9]. In Refs. [10,11] the tunneling probability through a CNT junction is modeled using a rectangular potential barrier and the quasiclassical approximation.

The authors of Ref. [12] employed an oversimplified two-parameter expression for contact resistance, with these parameters fitted to the experimental data. The best microscopic attempt, that we are aware of, is using the semiphenomenological tight-binding approximation for the calculations of contact resistance [13]. But in Ref. [13] just the microscopic part of the nanocomposites conductivity problem is addressed, and the conductivity of nanocomposite is not calculated. Moreover, in Ref. [13] the coaxial CNTs configuration is only considered, which is hardly realistic for real polymers.

Thus, the majority of investigations are concentrated on the mesoscopic part of the task: refining a percolation model or phenomenologically taking into account different geometry peculiarities of CNTs junctions. Moreover, comparison with experiments is missing in some publications on this topic. Thus, a truly multiscale investigation, capable of providing quantitative results comparable with experiments, combining fully first-principles calculations of contact resistance on the microscopic level with a percolation model on the mesoscopic level seems to be missing.

In our previous research [14], we proposed an efficient and precise method for fully first-principles calculations of CNTs contact resistance and combined it with a Monte-Carlo statistical percolation model to calculate the conductivity of a simplified example network of CNTs junctions without polymer filling. In the current paper, we are applying the developed approach to the modeling of conductivity of the CNTs enhanced polymer polyimide R-BAPB.

R-BAPB (Fig. 1) is a novel polyetherimide synthesized using 1,3-bis-(3′,4-dicarboxyphenoxy)-benzene (dianhidride R) and 4,4′-bis-(4″-aminophenoxy)diphenyl (diamine BAPB). It is thermostable polymer with extremely high thermomechanical properties (glass transition temperature $T_g = 453$–463 K, melting temperature $T_m = 588$ K, Young's modulus $E = 3.2$ GPa) [15]. This polyetherimide could be used as a binder to produce composite and nanocomposite materials demanded in shipbuilding, aerospace, and other fields of industry. The two main advantages of the R-BAPB among other thermostable polymers are thermoplasticity and crystallinity. R-BAPB-based composites could be produced and processed using convenient melt technologies.

Crystallinity of R-BAPB in composites leads to improved mechanical properties of the materials, including bulk composites and nanocomposite fibers. It is well known that carbon nanofillers could act as nucleating agents for R-BAPB, increasing the degree of crystallinity of the polymer matrix in composites. As it was shown in experimental and theoretical studies [16–19], the degree of crystallinity of carbon nanofiller enhanced R-BAPB may be comparable to that of bulk polymers.

Ordering of polymer chains relative to nanotube axes could certainly influence the conductance of the polymer-filled nanoparticle junctions. However, it is expected that such influence will depend on many parameters, including the structure of a junction, position, and orientation of chain fragments on the nanotube surface close to a junction, and others. Taking into account all of these parameters is a rather complex task that requires high computational resources for atomistic modeling and *ab initio* calculations, as well as complex analysis procedures. Thus, on the current stage of the study, we consider only systems where the polymer matrix was in an amorphous state, i.e., no sufficient polymer chains ordering relative to nanotubes were observed.

The ultimate goal of the efforts aimed at the modeling of nanocomposites conductivity would be a model parameterized with the different geometrical parameters of the polymer-nanotubes system. Those geometrical parameters include CNTs type, CNTs overlap length, the distance between CNTs, CNTs crossing angles, and possible presence of defects in CNTs. The mentioned peculiarities affect composites conductivity to varying degrees. As was shown in our previous work ([14]) probably the most significant geometrical factor leading to variations in the junctions contact resistance is the CNTs crossing angles and the distance between CNTs. Also to some degree, the contact resistance may depend on CNTs chirality (which determines whether CNTs are metallic or semiconducting and CNTs size) and CNTs overlap length. In the current work, we investigate in detail the contact resistance of CNTs configurations filled with polymers that differ in crossing angle and distance between CNTs. At the same time, the influence of CNTs overlap and chirality is investigated using just CNTs, without polymer.

II. DESCRIPTION OF THE MULTISCALE PROCEDURE

The modeling of polymer nanocomposite electrical conductivity is based on a multiscale approach, in which different simulation models are used at different scales. For the electron transport in polymer composites with a conducting filler, the lowest scale corresponds to the contact resistance between

tubes. The contact resistance is determined at the atomistic scale by tunneling of electrons between the filler particles via a polymer matrix, and hence, analysis of contact resistance requires knowledge of the atomistic structure of a contact. Therefore, at the first step, we develop an atomistic model of the contact between carbon nanotubes in a polyimide matrix using the molecular dynamics (MD) method. This method gives us the structure of the intercalated polymer molecules between carbon nanotubes for different intersection angles between the nanotubes. One should mention that since a polymer matrix is soft, the contact structure varies with time, and, therefore, we use molecular dynamics to sample these structures.

Based on the determined atomistic structures of the contacts between nanotubes in the polymer matrix we calculate electron transport through the junction using electronic structure calculations and the formalism of the Green's matrix. Since this analysis requires first-principles methods, one has to reduce the size of the atomistic structure of a contact to acceptable values for the first-principles methods, and we developed a special procedure for cutting the contact structure from MD results. First-principles calculations of contact resistance should be performed for all snapshots of an atomistic contact structure of MD simulations, and an average value and a standard deviation should be extracted. In this way, one can get the dependence of contact resistance on the intersection angle and contact distance.

Using information about contact resistances we estimate the macroscopic conductivity of a composite with nanotube fillers. For this, we used a percolation model based on the Monte Carlo method to construct a nanotube network in a polymer matrix. In this model, we used distributions of contact resistances, obtained from the first-principles calculations for the given angle between nanotubes. Using this Monte Carlo percolation model one can investigate the influence of nonuniformities of a nanotube distribution on macroscopic electrical conductivity.

In the A section, we will describe the details of molecular dynamics modeling of the atomistic structure of contacts between nanotubes. In the B section, we present the details of first-principles calculations of electron transport for estimates of contact resistance. Finally, in the C section, we present the details of the Monte Carlo percolation model.

A. Preparation of the composite atomic configurations

Initially, two metallic CNTs with chirality (5,5) were constructed and separated by 6 Å. The CNTs consisted of 20 periods along the axis, and each one had a total length of 4.92 nm. The broken bonds at the ends of the CNTs were saturated with hydrogen atoms. The distance 6 Å was chosen, because starting with this distance polymer molecules are able to penetrate the space between CNTs. The three configurations of CNTs junctions were prepared: the first one with parallel CNTs axes (angle between nanotube axes $\varphi = 0^\circ$), the second one with the axes crossing at 45 degrees ($\varphi = 45^\circ$), and the third one with perpendicular axes ($\varphi = 90^\circ$).

To produce the polymer-filled samples, we used a procedure similar to that employed for the simulations of the thermoplastic polyimides and polyimide-based nanocomposites in the previous works [17,18,20–24]. First, partially coiled R-BAPB chains with the polymerization degree $N_p = 8$, which corresponds to the polymer regime onset [21,22], were added to the simulation box at random positions avoiding overlapping of polymer chains. This results in the initial configuration of samples with a rather low overall density ($\rho \sim 100\,\mathrm{kg/m^3}$) (Fig. 2). Then the molecular dynamics simulations were performed to compress the systems generated, equilibrate them, and perform production runs.

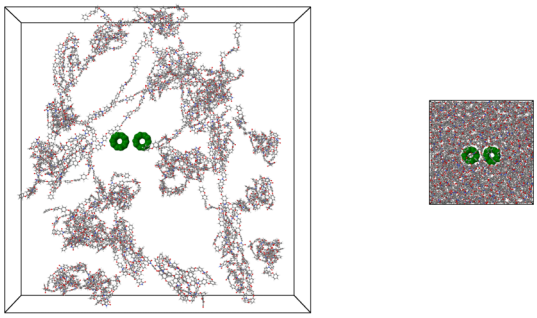

FIG. 2. The snapshots of the nanocomposite system with the parallel orientation of carbon nanotubes at the initial state (left frame) and after the compression procedure (right frame). The black lines represent the periodic simulation cell.

The molecular dynamics simulations were carried out using Gromacs simulation package [25,26]. The atomistic models used to represent both the R-BAPB polyimide and CNTs were parameterized using the Gromos53a6 force field [27]. Partial charges were calculated using the Hartree-Fock quantum-mechanical method with the 6-31G* basis set, and the Mulliken method was applied to estimate the values of the particle charges from an electron density distribution. As was shown recently, this combination of the force field and particle charges parametrization method allows one to reproduce qualitatively and quantitatively the thermophysical properties of thermoplastic polyimides [20]. The model used in the present work was successfully utilized to study structural, thermophysical, and mechanical properties of the R-BAPB polyimide and R-BAPB-based nanocomposites [17,18,20–22].

All simulations were performed using the NpT ensemble at temperature $T = 600$ K, which is higher than the glass transition temperature of R-BAPB. This temperature was chosen to make the equilibration of the polymer more rapid. As the experimental evidence shows [28,29], the conductivity of CNTs enhanced polymers does depend on temperature, but this dependence becomes less significant at the temperatures above 200 K. As the temperature approaches 300 K, the changes in conductivity become practically negligible. Thus, the temperature $T = 600$ K is used for the rapid thermal equilibration and obtaining production configurations, and the results for conductivity will be valid for temperatures above 300 K. The temperature and pressure values were maintained using Berendsen thermostat and barostat [30,31] with relaxation times $\tau_T = 0.1$ ps and $\tau_p = 0.5$ ps, respectively. The electrostatic interactions were taken into account using the particle-mesh Ewald summation (PME) method [32,33].

The step-wise compression procedure allows one to obtain dense samples with an overall density close to the

experimental polyimide density value ($\rho \approx$ 1250–1300 kg/m^3), as shown in Fig. 2. The system pressure p during compression was increased in a stepwise manner up to $p = 1000$ bar and decreased then to $p = 1$ bar. After compression and equilibration, the production runs were performed to obtain the set of polymer-filled CNT junction configurations.

As the conductance of polymer-filled CNT junctions is influenced by the density and structure of a polymer matrix in the nearest vicinity of a contact between CNTs, the relaxation of the overall system density was used as the system equilibration criterion. To estimate the equilibration time, the time dependence of the system density was calculated as well as the density autocorrelation function $C_\rho(t)$:

$$C_\rho(t) = \frac{\langle \rho(0)\rho(t)\rangle}{\langle \rho^2\rangle}, \tag{1}$$

where $\rho(t)$ is the density of the system at time t and $\langle \rho^2\rangle$ is the average density of the system during the simulation.

As shown in Fig. 3(a), the system density does not change sufficiently during simulation after the compression procedure. At the same time, the analysis of the density autocorrelation functions shows some difference in the relaxation processes in the systems studied [see Fig. 3(b)]. In the case of the system where CNTs were placed parallel to each other ($\varphi = 0^\circ$), $C_\rho(t)$ could be approximated by the exponential decay function $C_\rho(t) = \exp(-t/\tau)$ with relaxation time $\tau = 4$ ps. The density relaxation in the systems with crossed CNTs ($\varphi = 45^\circ$ and $\varphi = 90^\circ$) was found to be slower. For these two systems density the autocorrelation functions could be approximated by a double exponential function $C_\rho(t) = A\exp(-t/\tau_1) + (1-A)\exp(-t/\tau_2)$, and the relaxation times determined using this fitting were $\tau_1 = 2.7$ ps and $\tau_2 = 12.2$ ns (for $\varphi = 90^\circ$) and $\tau_1 = 9.5$ ps and $\tau_2 = 24.6$ ns (in case of $\varphi = 45^\circ$).

Also we have calculated time autocorrelation functions $C_\theta(t) = \langle \cos[\theta(\tau) - \theta(\tau + t)]\rangle_\tau$ for dihedral angles θ in both dianhydride and diamine parts of the R-BAPB monomer unit and estimated corresponding relaxation times to characterize relaxation of local mobility of polymer chains in the systems considered. The angles chosen to calculate relaxation characteristics are of the same nature and correspond to the rotation around O-C_{Ar} bonds. These angles are shown by thick bonds in the R-BAPB structure (Fig. 1). The characteristic relaxation times τ_θ were obtained by fitting $C_\theta(t)$ using the Kohlrausch "Williams" Watts (KWW) stretched exponentials $C_\theta(t) = A\exp(-(t/\tau_\theta)^\beta)$, where $A \leqslant 1$, and β is the stretching parameter taking into account the nonexponentiality of the relaxational process. It was shown that for all systems considered autocorrelation functions $C_\theta(t)$ drop to values close to zero on 250 ns timescale, Fig. 3(c). The characteristic relaxation times estimated by fitting of the autocorrelation functions were $\tau_\theta = 10.9$ ns in the case of $\varphi = 0^\circ$, $\tau_\theta = 11.8$ ns ($\varphi = 90^\circ$), and $\tau_\theta = 37.7$ ns ($\varphi = 45^\circ$).

The results obtained after the analysis of the system density relaxation allow us to choose the system equilibration time to be 100 ns, which is higher than the longest system density relaxation times determined by the density autocorrelation function analysis. Calculation of relaxation characteristics

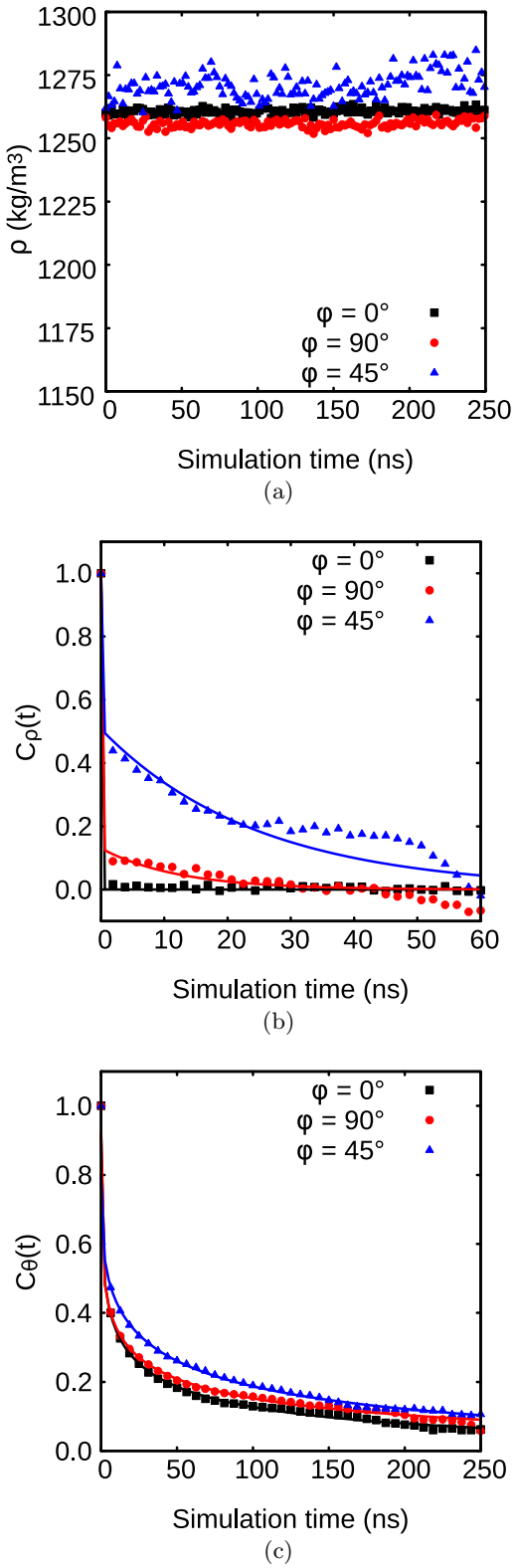

FIG. 3. The time dependence of the system density ρ (a), the density autocorrelation functions $C_\rho(t)$ (b), and the dihedral angle autocorrelation function $C_\theta(t)$ (c) for the systems with various angles between nanotube axes φ. The dots correspond to the calculated data. The solid lines correspond to the fitting of $C_\rho(t)$ with the exponential (in case of $\varphi = 0^\circ$) or double exponential (in case of $\varphi = 45^\circ$ and $\varphi = 90^\circ$) functions, and to the fitting of $C_\theta(t)$ using KWW stretched exponentials.

of dihedral angles in R-BAPB polymer chains confirms our conclusion that we achieve local relaxation of polymer conformations during 100 ns of MD simulations. The same simulation time was used in our previous works to equilibrate the nanocomposite structure after switching on electrostatic interactions [17,20,24]. The equilibration was followed by the 150 ns long production run. To analyze the polymer-filled CNT junction conductance, 31 configurations of each simulated system, separated by 5 ns intervals, were taken from the production run trajectory.

After the configurational relaxation is finished, we have to prepare atomic configurations for polymer-filled CNT junctions for the first-principles calculations of contact resistance. The method we used for the calculations of contact resistance is based on the solution of the ballistic electronic transport problem, finding the volt-ampere characteristic $I(V)$ of a device and deriving the contact resistance from the linear part of $I(V)$ corresponding to the low voltages. For this purpose, we employed the Green's function method for solving the scattering problem and the Landauer-Buttiker approach to find the current through a scattering region coupled to two semi-infinite leads, as described in Ref. [34]. Specific details of how these techniques are applied in the case of crossed CNTs can be found in Ref. [14].

B. The first-principles calculations of the contact resistance of CNTs junctions filled with polymer

For the preparation of a device for the electronic transport calculations, we first form that part of the device which consists of the atoms belonging to the CNTs used in the CNTs plus polymer relaxation. Regions with the same geometry as in Ref. [14] are cut from the initial 20-period long CNTs, and the rest of the atoms belonging to the CNTs are discarded. This is done to make possible a direct comparison of the results obtained for the polymer-filled CNTs junctions with the results for CNTs junctions without polymer reported in Ref. [14] for the same separation of CNTs equal to 6 Å.

Note that the CNTs parts of the scattering device contain atoms shifted from their positions in ideal CNTs due to the influence of the adjacent polymer molecules, and these shifts are time dependent as a result of differences in local polymer configuration.

The cut regions contain two fragments of CNTs each 9 periods long, and in the case of the CNTs parallel configuration, the CNTs overlap by 7 periods. In the nonparallel configurations, one of the CNTs is rotated around the axis perpendicular to the CNTs axes in the parallel configuration and passing through the geometrical center of a device in the parallel configuration. After the construction of the CNTs part of the scattering region, we attach to it leads that consist of 5 period long fragments of an ideal CNT. The CNTs parts of the scattering regions with the attached leads for the three considered configurations are shown in Fig. 4.

For the convenience of the reader we remind here the basic terminology used in the field of electronic quantum transport at the microscale. An atomic configuration for calculations of the quantum transport at the microscale consists of a central scattering region and semi-infinite leads that serve as sources of carriers. In Figs. 4 and 5 the leads are green and the rest of

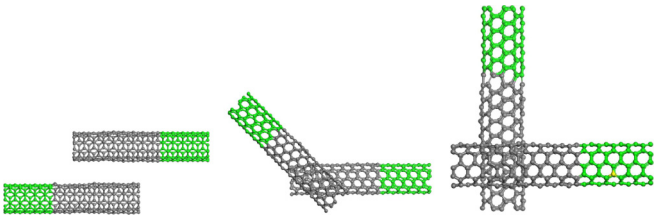

FIG. 4. The CNTs parts of the junctions. Left: the parallel configuration, center: CNTs axes are crossing at 45 degrees, right: the perpendicular configuration. The leads atoms are colored by green.

the atoms belong to the central scattering region. Note that only single periods of the leads are represented in Figs. 4 and 5. These single periods are repeated semi-infinitely in the directions from the central scattering regions. A central scattering region together with semi-infinite leads is called a "whole device" or just a "device." A device may contain a different number of atoms as shown below.

After the preparation of the CNT parts of the junctions, we still have 17 766 atoms in a device. A system with such a large number of atoms cannot be treated by fully first-principles atomistic methods. On the other hand, keeping all those atoms for a precision calculation of the contact resistance of polymer-filled CNTs junctions is not necessary, as only those polymer atoms which are close enough to a CNT will serve as tunneling bridges and give a contribution to the junctions conductivity. Thus, for the calculations of the contact resistance, only those atoms were kept which are closer to the CNTs than a certain distance d. It has been established by numerical experiments that if the value of d is taken equal to the CNTs separation $d = 6$ Å this is quite sufficient, and taking into account more distant atoms does not change the contact resistance significantly.

The procedure of sorting the polymer atoms is as follows. In our molecular dynamics simulations, we used 27 separate polymer molecules, consisting of eight monomers each. If at least one of the atoms of a polymer molecule was closer to the CNTs part of a junction than $d = 6$ Å, the whole molecule was kept for a while and discarded otherwise. Having applied this first part of the procedure, we kept four polymer molecules for the parallel configuration, eight molecules for

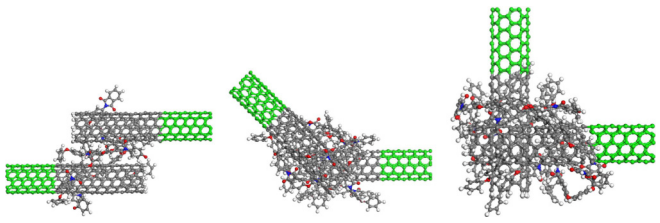

FIG. 5. The atomic configurations for the first-principles calculations of the polymer filled CNTs junctions contact resistance. The configurations are for the first time steps in the corresponding series. Left: the parallel configuration, center: CNTs axes are crossed at 45 degrees, right: the perpendicular configuration. The carbon atoms are gray, the nitrogen atoms are blue, the oxygen atoms are red, and the hydrogen atoms are light gray. The leads atoms are colored in green.

the perpendicular configuration, and 11 molecules for the 45 degrees configuration.

Then we looked at the polymer molecules that satisfied the criterion used in the first round of selections. The same procedure was applied to monomers as the one used earlier for molecules: If at least one of the monomer atoms was closer to the CNTs part of a junction than $d = 6$ Å, the whole monomer was kept for a while and discarded otherwise.

After the second round of selection with monomers was over, we dealt in the same manner with the individual residues comprising a monomer. The broken bonds that appeared in the second and third stages were saturated with hydrogen atoms. The described procedure resulted in the following numbers of atoms in the whole device, including the central scattering region and the leads: 881 for the parallel configuration, 1150 for the perpendicular configuration, and 1074 for the 45 degrees configuration. The atomic configurations obtained using the described procedure for the first time steps in the corresponding series are presented in Fig. 5.

A fully *ab initio* method for electronic structure investigations utilizing a localized pseudoatomic basis set, as described in Ref. [35] and implemented in Ref. [36], was used for the calculations of the electronic structures of the whole device and the leads. We used basis set s2p2d1, the pseudoatomic orbitals (PAO) cutoff radius equal to 6.0 a.u., and the cutoff energy of 150 Ry. The pseudopotentials generated according to the Morrison, Bylander, and Kleinman scheme [37] were used. For the density functional calculations, the exchange-correlation functional was used in the PBE96 form [38].

Using the electronic structures of the whole device and the leads we calculated the energy-dependent transmission function through the device. Then the dependence $I(V)$ of the current I on the voltage V between the leads was determined with the Green's function approach as described in detail in Ref. [34]. Finally, the Landauer-Buttiker approach was used to find the current through a polymer-filled CNTs junction.

Solving a scattering problem for a nanodevice at arbitrary voltages is a computationally very complex task since it requires achieving self-consistency for both electron density and induced electrostatic potential simultaneously. Fortunately, for contact resistance calculations one can take advantage of the fact that the required voltages are very low.

According to the experimental evidence, the size of a nanocomposite specimen used in conductivity experiments is about 10 mm [39], and the typical voltages applied across such specimen do not exceed 100 V [40]. The characteristic size of the scattering regions (the parts of the atomic configurations between the green leads in Fig. 5) for the devices considered in this paper is about 1 nm in all directions. This corresponds to the voltage drop across a scattering region about 10^{-5} V, which is well within the range where the simplified approach is applicable, thus making our computational scheme relevant. The sizes of CNTs present in real polymers are larger approximately by one order of magnitude than the sizes of CNTs used in our calculations. Thus the voltage drop in real polymers is in the range from 10^{-4} V to 10^{-3} V, which is still within or close to the linearity area.

The question of the modeling of quantum transport in the limit of low voltages was discussed in detail in Ref. [14], where it was demonstrated that in the case of moderate voltages between leads, the scattering probability $T(E)$ is not sensitive to the details of the electrostatic potential distribution $V(\mathbf{r})$ in the central scattering region, and some physically reasonable approximation may be chosen for $V(\mathbf{r})$.

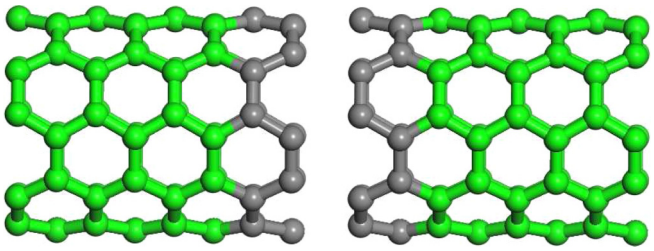

FIG. 6. The atomic configuration used in this work to validate the method of calculating quantum transport by comparing it against the consistent NEGF approach.

This is due to the fact that the difference of the Fermi functions $f(\varepsilon - \mu_L)$ and $f(\varepsilon - \mu_R)$ for the left and right leads with corresponding chemical potentials μ_L and μ_R, present in the original Landauer-Buttiker formula:

$$I = \frac{2e}{h} \int T(\varepsilon)(f(\varepsilon - \mu_L) - f(\varepsilon - \mu_R))d\varepsilon, \qquad (2)$$

where e is the elementary charge, h is the Planck constant, ε is the electron energy, and $T(\varepsilon)$ is the energy-dependent transmission probability, is reduced in this case to a very narrow and sharp peak centered at the Fermi level of the device.

In addition to the analysis performed in Ref. [14], in this paper, to verify the accuracy of our approach, we made contact resistance calculations for a simple test CNT junction in a coaxial configuration, using both the simplified method we suggest and the full NEGF method, where not only electron charge density but the electric potential was converged as well. The interlead voltage used in those test calculations was set to 10^{-4} V, and the gap between the CNTs tips was 0.94 Å. The atomic configurations for the test calculations are presented in Fig. 6. The consistent NEGF calculations produced 1.71×10^{-5} S for the conductance of the junctions shown in Fig. 6, while modeling without searching for convergence of potential yielded 1.72×10^{-5} S.

Thus, in our case, a very complex task of finding the $I(V)$ characteristic of a nanodevice can be significantly simplified without the loss of precision. For the $I(V)$ calculations in the current paper we employed the abrupt potential model introduced in Ref. [14]: The potentials V_L for the left lead and V_R for the right lead were set and were used for all atoms of the corresponding CNT to which that lead belonged. As for the polymer atoms, both V_L and V_R can be safely used for them, and at the considered voltages, adopting these two options, as we have checked by direct calculations, leads to the differences in current not exceeding 0.1%.

C. The percolation model

Determination of the conductivity of a polymer-CNT system can be implemented in two stages. First, a percolation cluster is formed, and the second stage implies solving the matrix problem for a random resistor circuit (network).

At the first stage, the modeling area—a cube of the linear size L—is filled with CNTs. For this task, permeable capsules (cylinders with hemispheres at the ends) with a fixed length and diameter were chosen as filling objects corresponding to CNTs. The cube is filled by the successive addition of CNTs until a fixed bulk density of CNTs

$$\eta = \frac{((4/3)\pi R^3 + \pi R^2 h)N}{L^3} \tag{3}$$

in the cube is reached, where R is the radius of the cylinder and hemisphere, h is the height of the cylinder, and N is the number of CNTs in the cube. The percolation problem for permeable capsules was previously solved in Ref. [41], and in Ref. [42] capsules with a semipermeable shell were considered.

In the percolation problem, we use periodic boundary conditions as, for example, in Ref. [10]. We use the method of finding a percolation threshold based on the Newman and Ziff algorithm [43], where the identification of a percolation cluster is made at the stage of its formation. When a percolation cluster is formed, the obtained CNT configuration is transformed into a resistor circuit (second stage).

The contributions to a conductance matrix resulting from the inner resistance of CNTs and the tunneling resistance of junctions are usually discussed in connection with constructing conductivity percolation algorithms. Direct measurements of CNTs resistance per unit length are available. In Ref. [44], the inner resistance of CNTs is estimated as $15 \times 10^3\ \Omega/\mu$m. The results of Ref. [45] give specific CNTs resistance in the range $(12–86) \times 10^3\ \Omega/\mu$m. Taking into account that the characteristic CNTs lengths in nanocomposites are about several μm [39,40], this results in the inner CNTs resistance approximately 10^4–$10^5\ \Omega$, which is at least one order of magnitude less than the tunneling resistance obtained in this work. The specific results on tunneling resistance will be discussed below in Sec. III. Thus, in our percolation model, the inner resistance of CNTs is neglected, and only the tunneling resistance of CNTs junctions is taken into account. This can significantly reduce the requirements for computational time.

When contact resistance is determined only by tunneling, the principle of compiling the matrix for the percolation problem, after a percolation cluster has been identified, will be as follows. First, the matrix (N, N) is compiled from the bonds of percolation elements, where N is the number of CNTs participating in percolation. Then this matrix is filled with the values of the conductance of the polymer-filled CNTs junctions G_{ij}. The matrix elements G_{ij} are calculated using a precise quantum mechanical approach taking into account the crossing angle between CNTs. Since the position and direction of every filler used in the percolation problem are known, one can calculate a crossing angle for every junction that is a part of a percolation cluster and use the value of G_{ij} corresponding to this angle. How a specific value of G_{ij} is assigned to a particular junction is described in detail below in Sec. III. Finally, the components V_k of the voltage vector $\mathbf{V}$ corresponding to the kth contact point in a percolation network are determined according to the second Kirchhoff law [46].

$$\sum_j G_{ij}(V_i - V_j) = 0; \tag{4}$$

the sum of currents for all internal elements of a percolation network is zero. The voltages on the left and right borders of a simulation volume are set to $V_L = 1$ V and $V_R = 0$ V, respectively.

Now finding the conductivity of the system is reduced to the problem $\mathbf{GV} = \mathbf{I}$, where $\mathbf{G}$ is the conductance matrix and $\mathbf{I}$ is the vector of the currents between the contact points.

After solving equation (4), with the elements of the $\mathbf{G}$ matrix obtained by the first-principles calculations, we obtain the voltage vector for all internal elements. Then, knowing this vector, we sum up all the currents on each of the boundaries. The currents on the left I_L and right I_R boundaries of a simulation volume are equal in magnitude and opposite in sign $I_L = -I_R$. Knowing these currents, we determine the conductance of the simulation system as $G = |I_L|/(V_L - V_R) = |I_R|/(V_L - V_R)$. Then the conductivity of the composite is calculated as $\sigma = GL/S$, where L is the distance between the faces of a simulation volume where voltage is applied, and S is the area of that kind of face. In our case, for the simulation volume of a cubic shape, $S = L^2$, and $\sigma = G/L$.

To calculate the conductivity, the following system parameters were selected: The length of a nanotube is $l = 3\ \mu$m, the diameter of a CNT is $D = 30$ nm, the aspect ratio $l/D = 100$, and the size of the system is $4\ \mu$m. The same values were used in Ref. [6]. We adopted those values to test our realization of the percolation algorithm against the previously obtained results [6]. Then for the given parameters for each fixed tube density, the Monte Carlo method (100 implementations of various configurations of CNT networks) was used to calculate the system conductivity. The quality of CNTs dispersion is one of the key factors that affect the properties of nanocomposites, and a lot of effort is taken to achieve a homogeneous distribution of fillers in regular polymers [47].

On the other hand, there are some special cases when fillers self-assembly in a particular manner enhances the properties of composites compared to the homogeneous distributions of fillers. These cases include the composites based on the specific polymers. For example, in Ref. [48] a multicomponent polymer undergoing phase separation is modeled. The carbon fillers in that polymer are agglomerated in the minority phase. In Ref. [49] a block copolymer that has a sandwichlike layered structure is considered, and the carbon nanorods are aligned in the layers of one type. In Ref. [50], the CNTs are located in a thin layer near the surface of the polymer.

In our case, the R-BAPB polyimide polymer does not exhibit any of the peculiarities discussed in Refs. [48–50]. However, those peculiarities can be incorporated into the proposed multiscale procedure by just distributing CNTs in some specific manner when forming a percolation cluster. Doing that, the information on the distribution of the fillers from Refs. [48–50] can be used as an input for the multiscale procedure proposed in this work. The other two steps: equilibrating a polymer and calculating contact resistances remain unchanged.

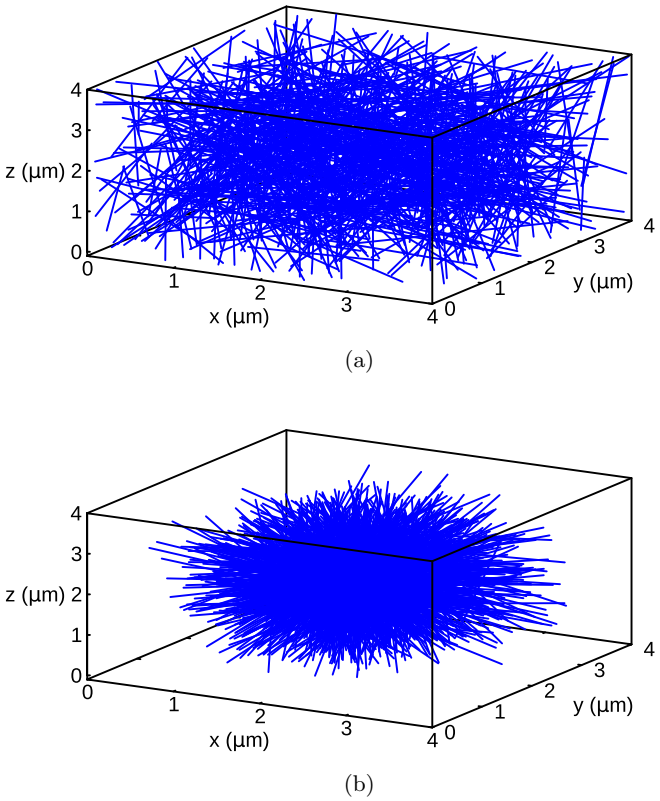

FIG. 7. The uniform (a) and agglomerated with $\rho_\sigma = L/12$ (b) distributions of CNTs in the simulation volume.

In this work, we take into consideration the effect of inhomogeneity of a CNTs distribution on composite conductivity. The spatial density of nanotubes ρ_{CNT}, in this case, has one peak with a Gaussian distribution:

$$\rho_{\mathrm{CNT}} = \rho_0 \cdot \exp(-(\mathbf{r} - \mathbf{r_0})^2/\rho_\sigma^2), \tag{5}$$

where $\mathbf{r}_0$ coincides with the geometrical center of a simulation volume, and $\rho_\sigma = L/12$. The value of the ρ_0 parameter is chosen so that the CNTs volume fraction in the inhomogeneous case is the same as in the homogeneous distribution. The uniform and agglomerated distributions of CNTs are shown in Fig. 7.

III. RESULTS AND DISCUSSION

To find the contact resistance of polymer filled CNTs junctions one first needs to find their volt-ampere characteristics $I(V)$ and to determine the voltage range where $I(V)$ is linear and is not sensitive to the specific distribution of the electrostatic potential in the scattering region. In Fig. 8 the $I(V)$ plot for the first time step in the atomic geometry series for the parallel configuration is shown.

It is clearly seen from Fig. 8 that up to about 10^{-4} V the $I(V)$ characteristic is linear, and after that value, it starts to deviate from a simple linear dependence. Thus, for the calculations of a contact resistance R and its inverse, a junction conductivity G, we used the electrical current values obtained for the interlead voltage equal to 10^{-4} V. Note that according to our estimates in Sec. II B, a characteristic voltage drop on

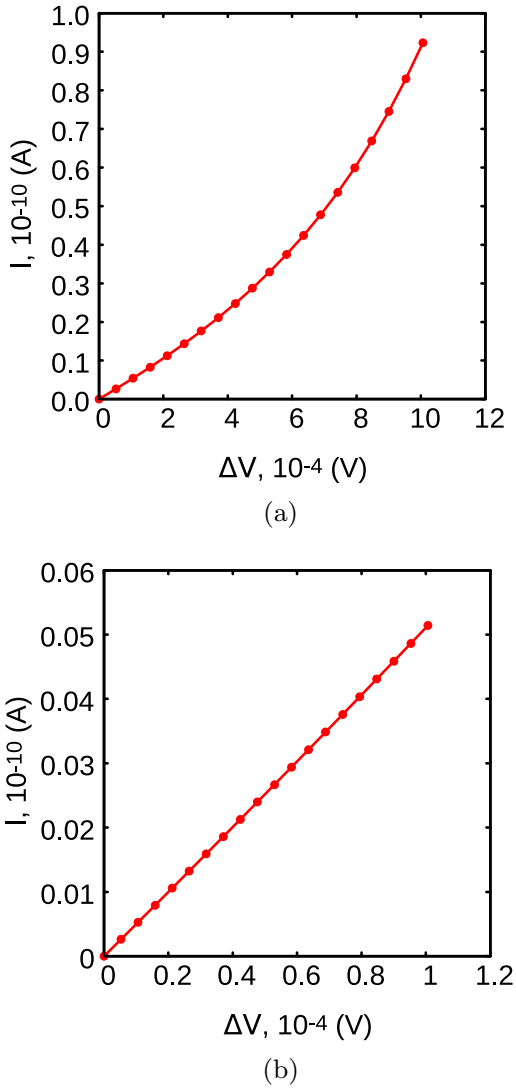

FIG. 8. The volt-ampere characteristic for the polymer filled CNTs junction corresponding to the first time step in the series for the parallel configuration. (a) Maximum interlead voltage is 10^{-3} V, (b) 10^{-4} V. The circles correspond to the results of calculations; the lines are guides for the eye.

the length of a CNTs tunneling junction is about 10^{-5} V which is well within the region where the linear $I(V)$ is observed.

The time dependences of the junctions conductances for the three considered configurations are presented in Fig. 9. One might expect that the shifts of both CNTs atoms and polymer atoms in the central scattering region due to thermal fluctuations would lead to fluctuations of junctions conductances G, but quantitative characteristics of this phenomenon such as minimum G_{min}, maximum G_{max}, mean values $\langle G \rangle$, and a standard deviation G_σ can only be captured by highly precise fully atomistic first-principles methods, like those employed in the current paper. The resulting fluctuations of conductance are very high. For the parallel CNTs configuration the minimum value, $G_{\mathrm{min}} = 2.4 \times 10^{-8}$ S, and the maximum value, $G_{\mathrm{max}} = 6.8 \times 10^{-6}$ S, differ by more than two orders of magnitude; for the 45 degrees and perpendicular configurations the corresponding ratios are about 30. These

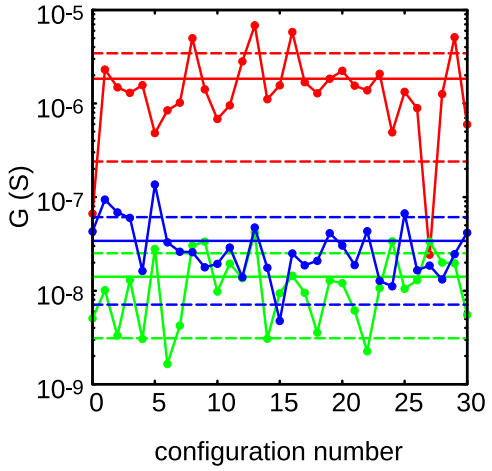

FIG. 9. The time dependence of the conductance of the polymer-filled junctions G in S for the separation between CNTs equal to 6 Å. The red color corresponds to the parallel configuration, the green lines to the perpendicular configuration, and the blue lines to the 45 degrees configuration. The results of the calculations are shown by circles, the saw-tooth lines serve as a guide for the eye. The straight solid lines designate the mean values of conductance $\langle G\rangle$ and the dashed ones $\langle G\rangle \pm G_\sigma$.

fluctuations are mainly due to the differences in local polymer configuration. The distance between the CNTs in different snapshots changes just negligibly.

The same strong variations of conductance over time were reported in Ref. [13] for the coaxial CNTs configuration, where the results were obtained using a semiempirical tight-binding approximation. Thus, it is obvious that for the precise determination of the conductance of polymer-filled CNTs junctions one needs to use fully atomistic approaches, and phenomenological methods taking atomic configurations into account on the average are not reliable.

To assign a tunneling resistance to a polymer-filled CNT junction the following algorithm was used. First, for each junction that had to be used in the percolation algorithm, the crossing angle between CNTs was calculated using the positions and directions of the CNTs comprising this junction. The contact resistance corresponding to this value of the angle was calculated using the following interpolation algorithm. The mean values and standard deviations for CNTs tunneling resistances and conductances calculated for the different atomic configurations corresponding to the different time steps are known for $\varphi = 0, \pi/4$, and $\pi/2$. Analyzing Fig. 4 of Ref. [14], one can see that though an angle dependence of current and hence conductivity is a rather complex function, in the first approximation one can adopt a roughly piecewise linear character for this function with the minimum located at $\varphi = 0.25\pi$. Thus the logarithm of the mean value of conductance μ_φ for the generated φ was set by linear interpolation between the logarithms of the mean values of conductances for $\varphi = 0$ and $\varphi = \pi/4$ or $\varphi = \pi/4$ and $\varphi = \pi/2$ presented in Table I. The same algorithm was applied to finding the standard deviation values σ_φ for the generated φ. After the statistical parameters for the generated φ are estimated, the conductivity of the junction is set to a random number generated using the normal distribution with the parameters μ_φ and σ_φ.

In Ref. [14], the conductances were reported for the CNTs junctions with almost the same geometry as the CNTs parts of the devices considered in the current paper. The only difference between the configurations is that in this work the carbon atoms belonging to the CNTs part of the central scattering region are shifted somewhat from their equilibrium positions due to the interaction with polymer. The maximum values of those shifts along the x, y, and z coordinates lie in the range 0.2–0.5 Å. This gives us the possibility to directly compare the current results to the data from Ref. [14] and thus elucidate the influence of polymer filling on the conductance of junctions. The corresponding data and the results of a basic statistical analysis for the case of the polymer-filled junctions are provided in Table I.

First, as was expected, filling CNTs junctions with polymer creates carrier tunneling paths and increases junctions conductance by 6–7 orders of magnitude. Second, it is evident that the CNTs axes crossing angle is crucial for the junctions conductivity when a polymer is present as was the case without polymer [14]. At the same time, the sharp dependence of polymer-filled junctions conductance on the CNTs crossing angle is somewhat different from the analogous dependence for junctions without polymers. While in the latter case this dependence is sharply nonmonotonous, with a pronounced minimum at the angles around 0.25π, in the former case there is a significant difference between the conductance values for the parallel and nonparallel configurations, but the configurations with the angle φ between CNTs angles equal

TABLE I. The results of statistical analysis of the CNTs junctions conductances in S, for different values of CNTs separation and CNTs crossing angles φ, without polymer from Ref. [14], and with polyimide R-BAPB filling obtained in the current paper.

φ and CNTs separation, Å	No polymer, the results of Ref. [14]	Polymer present			
		$G_{\min}$	$G_{\max}$	$\langle G\rangle$	G_σ
0, 6	3.6×10^{-13}	2.4×10^{-8}	6.8×10^{-6}	1.8×10^{-6}	1.6×10^{-6}
0.2π, 6	1.4×10^{-14}				
0.25π, 6		4.8×10^{-9}	1.4×10^{-7}	3.4×10^{-8}	2.7×10^{-8}
0.3π, 6	1.2×10^{-14}				
0.5π, 6	4.2×10^{-14}	2.2×10^{-9}	4.3×10^{-8}	1.4×10^{-8}	1.1×10^{-8}
0, 7		2.8×10^{-9}	1.1×10^{-6}	1.8×10^{-7}	2.8×10^{-7}
0, 8		3.8×10^{-9}	1.2×10^{-6}	1.2×10^{-7}	2.2×10^{-7}

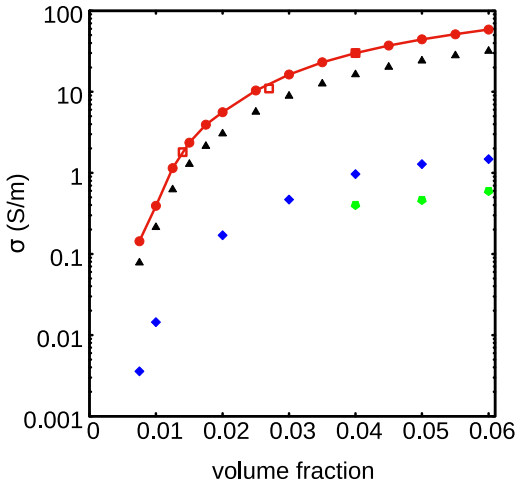

FIG. 10. The conductivity of CNT enhanced nanocomposites above the percolation threshold obtained in this work for the CNTs separation equal to 6 Å. The symbols of different shapes and colors are used to designate the following results. The red circles: the fixed CNTs tunneling junctions resistance of $R = 1$ MΩ is used, the red squares: the conductivity results for the fixed 1 MΩ tunneling resistance from Ref. [6], the black triangles: the same as the red circles but for $R = 0.54$ MΩ corresponding to the mean value of the tunneling junction resistance for the parallel configuration from Table I, the blue rhombi: the angle dependence of the CNTs junctions resistance is taken into account, the green pentagons: CNTs agglomeration is considered in addition to the angle dependence. The red line is a guide for the eye.

to 0.25π and 0.5π have very close conductances, and their mean values averaged over time $\langle G\rangle_{45}$ and $\langle G\rangle_{\rm per}$ lie within the ranges $\langle G\rangle \pm G_\sigma$ of each other. Moreover, in contrast to the geometries without polymer, for the polymer-filled CNTs junctions $\langle G\rangle_{\rm per}$ is lower than $\langle G\rangle_{45}$ by a factor of 2.4.

Note also that for the parallel configuration, the polymer influence on the junction conductance is more pronounced than for the nonparallel ones. For the parallel configuration, adding polymer to a junction of CNTs separated by 6.0 Å with initial conductance of 3.6×10^{-13} S produces a conductance mean value equal to 1.8×10^{-6} S. This gives the factor 0.5×10^7; the value of the analogous factor for the perpendicular configuration is 0.33×10^6.

The probable reason for the more effective conductance increase, when a polymer is added, for the configurations with smaller angles between CNTs axes, is that the smaller the intersection angle, the larger the overlap area between CNTs where a polymer can penetrate and thus create tunneling bridges. The higher fluctuation of conductance with time for the parallel configuration can be explained by the same reason: A larger CNTs overlap area gives more freedom for polymer atoms to adjust their positions.

The dependence of the calculated composite conductivity σ on CNTs volume fraction η $\sigma(\eta)$ is presented in Fig. 10. The value of the percolation threshold $\eta_{\rm thresh}$ is estimated in this work as $\eta_{\rm thresh} = 0.007$. To test our realization of the percolation algorithm against the previous results of Ref. [6] we calculated the composite conductivity using the fixed CNTs junction conductance equal to 1 MΩ for all junctions in a percolation network. Our results presented in Fig. 10 by the red circles coincide within graphical accuracy to the results of Ref. [6] shown by the red squares.

The 1 MΩ, used in various sources, for example Ref. [6], is not an arbitrary value but rather a typical contact resistance of CNTs junctions filled with polymer for simple geometries. In this work, we obtained for the parallel configurations $1/\langle G\rangle = 0.54$ MΩ. The $\sigma(\eta)$ dependence for the fixed tunneling resistance of 0.54 MΩ is shown in Fig. 10 by the black triangles.

Taking into account the angle dependence of CNTs junctions conductances with the statistical parameters according to Table I leads to the lowering of composite conductivity just above the percolation threshold by the factor of about 30. This number correlates with the ratio of the mean conductances for the parallel, $\langle G\rangle_{\rm par}$, and 45°, $\langle G\rangle_{45}$, configurations: $f_G = \langle G\rangle_{\rm par}/\langle G\rangle_{45} = 53$ but is lower than f_G due to the presence of junctions with $\varphi < \pi/4$.

The calculated conductivity of composite just above the percolation threshold without agglomeration at $\eta = 0.0075$ is equal to 3.6×10^{-3} S/m. This value is obtained with the fixed CNTs separation equal to 6 Å. The effect of varying the separation between CNTs on composites conductivity is discussed below.

If agglomeration of CNTs, modeled by the inhomogeneity of their distribution according to formula (5) and the parameter values discussed in Sec. II C, is taken into account in addition to the angle dependence of conductance, the composite conductivity is further reduced above a percolation threshold by the factor of 2.5. Lowering of conductivity of composites with agglomerated CNTs above a percolation threshold was also mentioned in Ref. [10]. The calculated results for the conductivity of a percolation network of agglomerated CNTs are shown in Fig. 10 by the green pentagons. Thus, taking into account agglomeration would shift the conductivity values just above the percolation threshold closer to 1.5×10^{-3} S/m.

Among the most important parameters that affect the contact resistance of CNTs junctions are the separation between CNTs and CNTs size. We have made direct calculations of contact resistances of CNTs junctions filled with polymers and the corresponding composite conductivities with separations between CNTs equal to 6.0 Å, 7.0 Å, and 8.0 Å. To save computational time, we have made calculations for the separations equal to 7.0 Å and 8.0 Å in parallel configurations only. The results are used to discuss the trends in conductivities as the separation between CNTs grows, which probably will be analogous for the other values of intersection angles.

As shown in Fig. 11, for the polymer volume fraction just above the percolation threshold, when the separation between CNTs is increased, first the composite conductivity becomes significantly lower—drops from 8.22×10^{-2} S for 6.0 Å to 8.26×10^{-3} S for 7.0 Å. If the separation is increased further, to 8.0 Å, the conductivity gets lower to a much less degree—4.50×10^{-3} S. Thus, then increasing separation between CNTs, the resulting composite conductivity tends to converge to some saturation value. In this case, two opposite tendencies are struggling: On one hand, with an increase in the distance between CNTs, the contact resistance increases; on the other hand, the increasing gap between CNTs allows the polymer to fill the distance between CNTs more uniformly.

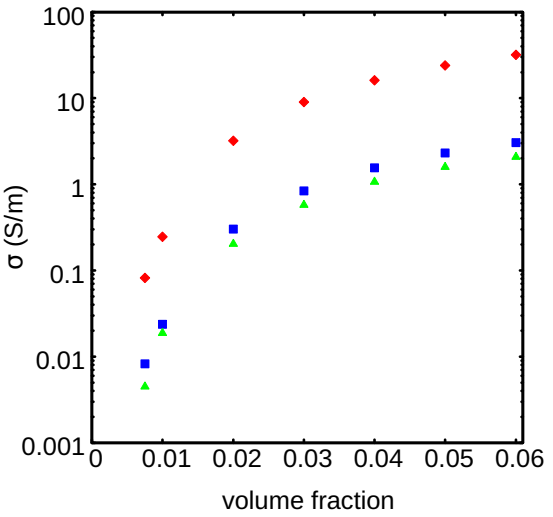

FIG. 11. The same as in Fig. 10 for the following configurations. The red rhombi—the mean value of the tunneling junction resistance for the parallel configuration with CNTs separation equal to 6.0 Å is used; the blue rhombi—the same as for the red rhombi, but the CNTs separation is 7.0 Å. The green rhombi—the same as for the red rhombi, but the CNTs separation is 8.0 Å.

In this case, starting from a certain distance between CNTs, apparently, the density of the polymer between CNTs reaches the density of the polymer in the region free of CNTs, and the efficiency of tunneling of charge carriers between CNTs is determined mainly by the properties of the polymer and not by the distance between CNTs. Thus, we have shown that by modeling the conductivity of contacts between CNTs at small distances between CNTs, it is possible by extrapolation to obtain estimates for the corresponding conductivities for realistic distances between CNTs. In this case, the conductivity value for the distance between CNTs equal to 8.0 is already quite close to the assumed limit. Thus to obtain the conductivity of a real polymer a Richardson extrapolation to a limit may be used [51]. If additionally to the trend in the dependence of conductivity on the separation between CNTs one takes into account the variations of junctions conductance with the CNTs crossing angle, the resulting conductivity of the composite is expected to lie between 10^{-4} S/m and 10^{-3} S/m.

The sizes of CNTs used in real polymers are significantly larger than the sizes for which precise quantum mechanical calculations are viable. On the other hand, microscopic first-principles calculations of contact resistance can only be fulfilled for configurations of relatively modest size.

Let us now discuss the effect of the size of CNTs on the resistance of contacts between CNTs. For this purpose, in addition to calculating the contact resistance for the $(5, 5) \times (5, 5)$ configuration, we calculated the contact resistance for the $(10, 10) \times (10, 10)$ configuration for the same distance between CNTs—6.0 Å.

Calculations of the contact resistance for CNT configurations $(5, 5) \times (5, 5)$ for a distance between CNTs of 6.0 Å, without a polymer, show that the result depends not only on the CNTs overlap length but also on the mutual angle of rotation of CNTs around their axes. Consider two configurations that differ in the rotation of CNTs around their axes. Sections of these two configurations by a plane perpendicular to the CNT axes are shown in Fig. 14. In the first configuration, let us call it "flat," the projections of the nearest bonds between carbon atoms in two adjacent CNTs are parallel. In the second configuration, let us call it "sharp," the projections of the nearest bonds are symmetric with respect to the vertical straight line passing through the centers of the CNT sections and thus form the maximum possible angles with the horizontal straight line. For the two configurations shown, the contact resistance differs by four orders of magnitude (see Table II).

This difference in conductivity is apparently due to the fact that in the "flat" configuration there are more atoms, the distances between which in neighboring CNTs are very close to the possible minimum, than for the "sharp" configuration. Similar calculations of the conductivity for "flat" and "sharp" configurations were also performed for intersections of CNTs with chirality $(10, 10) \times (10, 10)$. It was found that, as before, the conductivity for the "sharp" configuration is less than for the "flat" configuration. However, unlike CNTs with chirality (5,5), this difference is not four orders of magnitude but two times. This result seems physically reasonable, since with an increase in the radius of CNTs, the contact area between CNTs becomes locally more and more "flat," and the number of atoms in neighboring CNTs close to each other increases. An important result, in this case, is the fact that with an increase in the CNT radius with a change in chirality for a "flat" configuration, the conductivity changes only by a factor of 1.4. Consequently, one can expect convergence and reaching a certain conductivity limit with increasing CNT radius. Thus, the calculations of the conductivity of CNT aggregations performed for CNTs with small radii and small chirality indices can be used to estimate the conductivity of real composites, where the CNT radii are larger than those used in this work.

Note that the conductance of the polymer-filled junctions was calculated using "flat" configurations, as it is closer to the conductance of junctions between CNTs of larger diameter found in real polymers (Table II). Also, note that values of the conductances of the junctions with chiralities (5,5) and overlap length equal to seven periods in "flat" and "sharp" configurations are different from the value obtained in Ref. [14] and shown in Table I. This is due to the fact that the rotation of CNTs around their axes in Ref. [14] was arbitrary; no special care was taken to provide a specific orientation in this respect. Thus the value from Ref. [14] lies between the "flat" and "sharp" extremes closer to the value for the "flat" configuration.

The atomic configurations shown in Fig. 5 contain several hundred polymer atoms. Different groups of polymer atoms contribute to the conductivity of polymer-filled CNTs junctions to varying degrees. To identify the possible main tunneling bridges, we have performed the calculation of the junction conductance for the snapshot #15 of the parallel CNTs configuration with the separation between the CNTs equal to 7.0 Å keeping just one of the polymer chains. This snapshot was chosen because it has the largest conductance of all the other snapshots (1.15×10^{-6} S), and thus one can hope that a single polymer chain may give a major contribution to the conductance of the whole junction. The criterion for the

TABLE II. The conductances of the CNTs junctions without polymer for the parallel configurations with the separation between CNTs equal to 6 Å with various CNTs chiralities, sizes, and overlap lengths.

CNTs junctions geometry	Conductance (S)
(8, 0) × (8, 0)	3.66×10^{-11}
(8, 0) × (5, 5)	2.84×10^{-13}
(5, 5) × (5, 5), 3 periods overlap, "sharp"	1.42×10^{-17}
(5, 5) × (5, 5), 7 periods overlap, "sharp"	1.01×10^{-16}
(5, 5) × (5, 5), 11 periods overlap, "sharp"	2.03×10^{-16}
(5, 5) × (5, 5), 7 periods overlap, "flat"	1.30×10^{-12}
(10, 10) × (10, 10), 7 periods overlap, "flat"	1.86×10^{-12}
(10, 10) × (10, 10), 7 periods overlap, "sharp"	7.94×10^{-13}
(5, 5) × (5, 5), 7 periods overlap, "flat," COOH inside	3.62×10^{-8}
(5, 5) × (5, 5), 7 periods overlap, "flat," COOH outside	2.13×10^{-10}

choice of the chain is that it contains more atoms located inside the gap between CNTs than all other chains in the used atomic configuration. This atomic configuration is shown in Fig. 12. Indeed, the conductance of the junction with the chosen polymer chain is equal to 1.00×10^{-7} S which is two orders of magnitude above the minimum value for the set of the parallel configurations separated by 7.0 Å (2.81×10^{-9} S) and comparable to the mean value for this set (1.81×10^{-7} S). Thus, there exist groups of atoms that give major contributions to the conductance of junctions, but at the same time to obtain quantitative results one needs to carefully take into consideration all the atoms that are close enough to a junction.

When developing an algorithm for determining the polymer atoms that should be saved for calculating the conductivity of CNT junctions, we saved not only atoms in the gap between the CNTs but also atoms outside the gap. Of interest is the question of to what degree atoms outside the gap can affect the conductivity of polymer-filled CNT junctions. To answer this question, we performed calculations of CNT junctions functionalized with the hydroxyl group COOH. In one case, the hydroxyl group is located inside the gap between the CNTs, in the other—outside. The atomic configurations corresponding to the two cases are shown in Fig. 13. For the atoms of the hydroxyl group, together with the nearest CNT atoms, geometric optimization was performed.

As shown by the calculations (see Table II), the presence of a hydroxyl group in the gap between CNTs leads to an increase in the conductivity of CNT junctions by about a factor of 30 000. However, the presence of COOH outside the gap between CNTs also leads to a noticeable increase in conductivity—about 160 times. Thus, for an accurate determination of the conductivity of CNT junctions, one cannot completely neglect the polymer atoms located outside the gap between CNTs.

To investigate the influence of chirality of CNTs on CNTs' contact resistance, in addition to the configurations (5, 5) × (5, 5), we have calculated contact resistance for junctions of

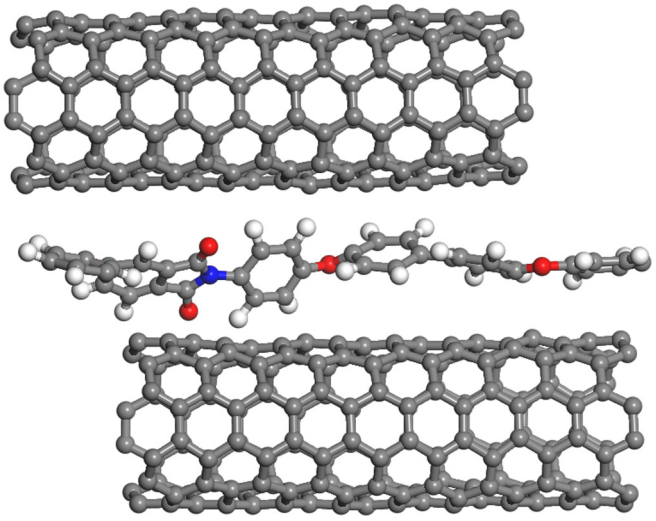

FIG. 12. The atomic configurations for the central scattering region (without leads) with the longest polymer chain inside the gap between the CNTs used for the illustration of the main tunneling bridge.

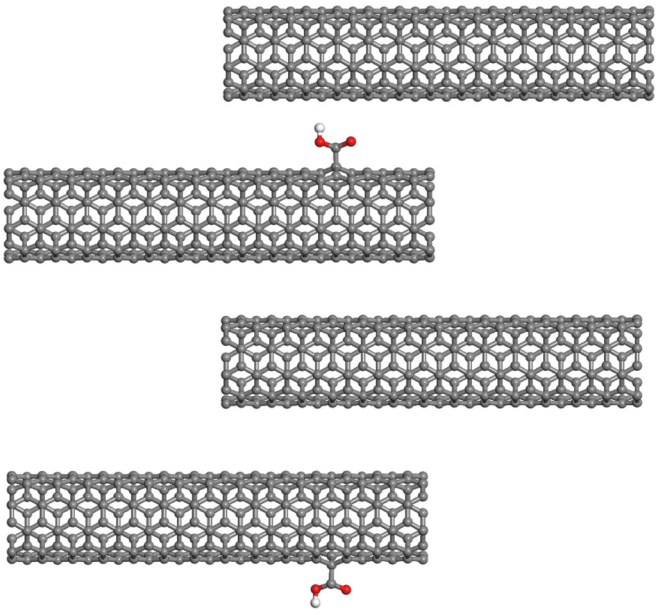

FIG. 13. The configuration of CNTs junctions functionalized by Hydroxyl group. Upper frame—the Hydroxyl group is inside the gap between CNTs. Lower frame—the Hydroxyl group is outside the gap.

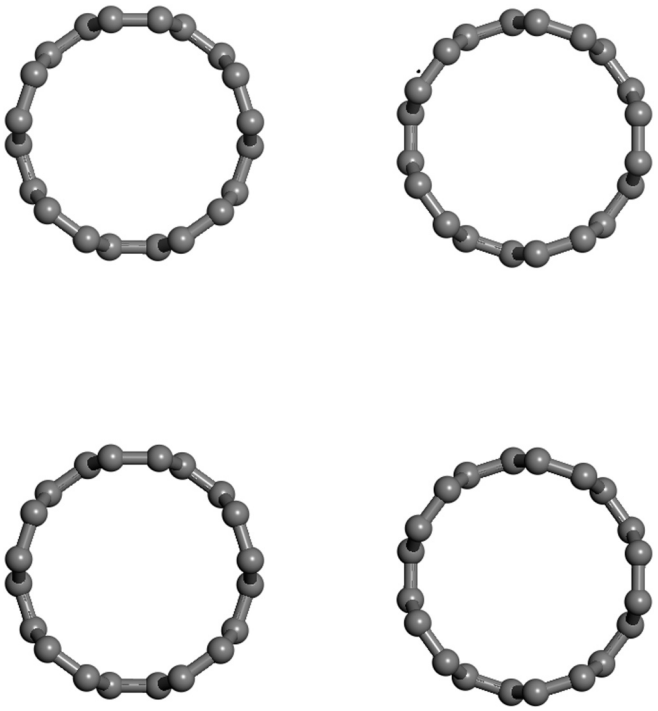

FIG. 14. A cross section view of the two configurations of the mutual orientation of parallel CNTs: the "flat" configuration (left) and the "sharp" configuration (right).

CNTs with chirality $(8, 0) \times (8, 0)$ and $(8, 0) \times (5, 5)$. The distance between CNTs for these calculations was taken as 6.0 Å and the overlap length is the same as for the $(5, 5) \times (5, 5)$ configurations with the overlap equal to seven periods. The results for those configurations are presented in Table II. As one can see from Table II, the chirality of CNTs does affect the conductance of CNTs junctions. The variations of conductance with chirality are about one order of magnitude and several orders of magnitude smaller than the characteristic conductances of the polymer-filled junctions. Thus the conductivity of composites is basically determined by the presence of a polymer intercalated between CNTs.

Let us now discuss a possible model of the dependence of the CNT conductivity junctions on the geometric parameters characterizing the mutual position of CNTs and their sizes. As can be seen from the calculations presented in this work (see Table II), with an increase in the distance between CNTs, there is a tendency for the contact resistance to saturate. Also, the contact resistance, with a sufficiently large CNT diameter, weakly depends on the CNT diameter. As the results of calculations presented in this work show, the dependence of the contact resistance of the intersection length of CNTs at a sufficiently large intersection length is almost linear. Significant deviations from the linear dependence arise when the length of the CNT intersection is less than seven periods or 1.7 nm. In fact, the fitting model for the dependence of the contact resistance of CNT junctions on the geometry should only contain the dependence of the contact resistance on the angle between the CNT axes. As discussed above, the dependence of the contact resistance on a given angle on a logarithmic scale can be approximated by a piecewise linear function.

Then the model for describing the dependence of the contact resistance G on the angle between CNTs axes φ can be presented using the following formula:

$$\lg(G(\varphi)) = \begin{cases} -\lg(\langle G\rangle_0)\dfrac{\varphi - \pi/4}{\pi/4} + \lg(\langle G\rangle_{45})\dfrac{\varphi}{\pi/4}, & 0 \leqslant \varphi \leqslant \pi/4; \\ -\lg(\langle G\rangle_{45})\dfrac{\varphi - \pi/2}{\pi/4} + \lg(\langle G\rangle_{90})\dfrac{\varphi - \pi/4}{\pi/4}, & \pi/4 \leqslant \varphi \leqslant \pi/2. \end{cases} \tag{6}$$

Thus, the strong angular dependence of the contact resistance is probably a consequence of the deviation from the linear dependence of the contact resistance on the length (and hence the intersection area of the CNTs). With an increase in the angle between CNTs, the area of intersection of CNTs decreases. At the same time, the situation when CNTs are strictly parallel, and the conductivity of the contact between them is proportional to the length of the overlap between the CNTs, is statistically rather rare. Consequently, it is not necessary to include such a linear dependence in the model describing the dependence of the conductivity of contacts on their geometry.

We believe that in this work we have identified some of the key factors that influence the electrical conductivity of nanocomposites: the geometry of tunneling junctions and changes of atomic configurations due to thermal fluctuations. Until the specific experiments on conductivity for R-BAPB polyimide are not available, we can make a preliminary comparison of our modeling results to the available experimental results for different composites. The calculated conductivity of composite just above the percolation threshold at $\eta = 0.0075$ is estimated to lie between 10^{-4} S/m and 10^{-3} S/m. This is a reasonable value that falls into the range of experimentally observed composites conductivities (for the comprehensive compilation of experimental results see Table 1 of Ref. [3]). To obtain a more quantitative value for the conductivity, computational efforts much more serious than those undertaken in the course of the preparation of this paper but still feasible are necessary.

IV. CONCLUSIONS

We have proposed a physically consistent, computationally simple, and at the same time precise, multiscale method for calculations of electrical conductivity of CNT enhanced nanocomposites. The method starts with the atomistic determination of the positions of polymer atoms intercalated between CNTs junctions, proceeds with the fully first-principles calculations of polymer-filled CNTs junctions conductance at the microscale, and finally performs modeling of percolation through an ensemble of CNTs junctions by the

Monte-Carlo technique. The developed approach has been applied to the modeling of electrical conductivity of polyimide R-BAPB plus single-wall CNTs nanocomposite.

Our major contributions to the field are the following. We have proposed a straightforward method to calculate a contact resistance and conductance for polymer-filled CNTs junctions with arbitrary atomic configurations without resorting to any simplifying assumptions. We have demonstrated that a consistent multiscale approach, based on solid microscopic physical methods can give reasonable results, lying within the experimental range, for the conductivity of composites and suggested a corresponding workflow.

It is shown that a contact resistance and nanocomposite conductivity is highly sensitive to the geometry of junctions, including an angle between CNTs axes and subtle thermal shifts of polymer atoms in an inter-CNT's gap. Thus, we argue that for the precision calculations of the electrical properties of nanocomposites rigorous atomistic quantum-mechanical approaches are indispensable.

Among the most important results of this work are the following. With an increase in the distance (the distances 6 Å, 7 Å, 8 Å are considered) between CNTs in the presence of a polymer, the value of the contact resistance reaches saturation. At a given distance between the CNT surfaces, the contact resistance with an increase in the CNT diameter from 6.78 Å [(5,5) chirality] to 13.56 [(10,10) chirality] weakly depends on the CNT size. Thus, calculations for small-diameter CNTs can be used to estimate the conductivity of contacts between CNTs found in real composites.

The estimated composite conductivity just above the percolation threshold is between 0.0001 and 0.001 S/m, which is within the experimental range for composites with various base polymers. Thus, the results of this paper demonstrate the possibility to model predictively the conductivity of CNTs enhanced polymers and provide the corresponding physical, mathematical, and computational procedures. The computational resources required to implement this procedure are viable using modern supercomputer equipment.

ACKNOWLEDGMENTS

This work was supported by the State Program "Organization of Scientific Research" (project 1001140) and by the Research Center "Kurchatov Institute" (order No. 2223 of 23/10/2020). This work has been carried out using computing resources of the federal collective usage center Complex for Simulation and Data Processing for Mega-science Facilities at NRC "Kurchatov Institute" [52].

[1] Yun-Ze Long, Meng-Meng, Changzhi Gub, Meixiang Wanc, Jean-Luc Duvaild, Zongwen Liue, and Zhiyong Fanf, Prog. Polym. Sci. **36**, 1415 (2011).
[2] G. B. Blanchet, C. R. Fincher, and F. Gao, Appl. Phys. Lett. **82**, 1290 (2003).
[3] A. V. Eletskii, A. A. Knizhnik, B. V. Potapkin, and J. M. Kenny, Phys.-Usp. **58**, 225 (2015).
[4] M. Soto, M. Esteva, O. Martínez-Romero, J. Baez, and A. Elías-Zúñiga, Materials **8**, 6697 (2015).
[5] S. Xu, O. Rezvanian, K. Peters, and M. A. Zikry, Nanotechnology **24**, 155706 (2013).
[6] Y. Yu, G. Song, and L. Sun, J. Appl. Phys. **108**, 084319 (2010).
[7] S.-H. Jang and H. Yin, Mater. Res. Express **2**, 045602 (2015).
[8] G. Pal and S. Kumar, Mater. Des. **89**, 129 (2016).
[9] J. T. Wescott, P. Kung, and A. Maitia, Appl. Phys. Lett. **90**, 033116 (2007).
[10] W. S. Bao, S. A. Meguid, Z. H. Zhu, and M. J. Meguid, Nanotechnology **22**, 485704 (2011).
[11] K. Grabowski, P. Zbyrad, T. Uhl, W. J. Staszewski, and P. Packo, Comput. Mater. Sci. **135**, 169 (2017).
[12] C. Micaela, R. Massimo, S. M. Imran, and T. Alberto, Composites: Part A **87**, 237 (2016).
[13] G. Penazzi, J. M. Carlsson, C. Diedrich, G. Olf, A. Pecchia, and T. Frauenheim, J. Phys. Chem. C **117**, 8020 (2013).
[14] K. Yu. Khromov, A. A. Knizhnik, B. V. Potapkin, and J. M. Kenny, J. Appl. Phys. **121**, 225102 (2017).
[15] V. E. Yudin, V. M. Svetlichyi, G. N. Gubanova, A. L. Didenko, T. E. Sukhanova, V. V. Kudryavtsev, S. Ratner, and G. Marom, J. Appl. Polym. Sci. **83**, 2873 (2002).
[16] V. E. Yudin, V. M. Svetlichnyi, A. N. Shumakov, D. G. Letenko, A. Y. Feldman, and G. Marom, Macromolecular Rapid Communications **26**, 885 (2005).
[17] S. V. Larin, S. G. Falkovich, V. M. Nazarychev, A. A. Gurtovenko, A. V. Lyulin, and S. V. Lyulin, RSC Adv. **4**, 830 (2014).
[18] S. G. Falkovich, S. V. Larin, A. V. Lyulin, V. E. Yudin, J. M. Kenny, and S. V. Lyulin, RSC Adv. **4**, 48606 (2014).
[19] V. E. Yudin, A. Y. Feldman, V. M. Svetlichnyi, A. N. Shumakov, and G. Marom, Compos. Sci. Tech. **67**, 789 (2007).
[20] V. M. Nazarychev, S. V. Larin, A. V. Yakimansky, N. V. Lukasheva, A. A. Gurtovenko, I. V. Gofman, V. E. Yudin, V. M. Svetlichnyi, J. M. Kenny, and S. V. Lyulin, J. Polym. Sci. B **53**, 912 (2015).
[21] S. V. Lyulin, A. A. Gurtovenko, S. V. Larin, V. M. Nazarychev, and A. V. Lyulin, Macromolecules **46**, 6357 (2013).
[22] S. V. Lyulin, S. V. Larin, A. A. Gurtovenko, V. M. Nazarychev, S. G. Falkovich, V. E. Yudin, V. M. Svetlichnyj, I. V. Gofman, and A. V. Lyulin, Soft Matter **10**, 1224 (2014).
[23] V. M. Nazarychev, A. V. Lyulin, S. V. Larin, I. V. Gofman, J. M. Kenny, and S. V. Lyulin, Macromolecules **49**, 6700 (2016).
[24] S. V. Larin, A. D. Glova, E. B. Serebryakov, V. M. Nazarychev, J. M. Kenny, and S. V. Lyulin, RSC Advances **5**, 51621 (2015).
[25] D. van der Spoel, E. Lindahl, B. Hess, G. Groenhof, A. E. Mark, and H. J. C. Berendsen, J. Comput. Chem. **26**, 1701 (2005).
[26] B. Hess, C. Kutzner, D. van der Spoel, and E. Lindahl, J. Chem. Theory Comput. **4**, 435 (2008).
[27] B. Hess, H. Bekker, H. J. C. Berendsen, and J. G. E. M. Fraaije, J. Comp. Chem. **18**, 1463 (1997).
[28] Y. Simsek, L. Ozyuzer, A. T. Seyhan, M. Tanoglu, and K. Schulte, Temperature dependence of electrical conductivity in double-wall and multi-wall carbon nanotube/polyester nanocomposites, J. Mater. Sci. **42**, 9689 (2007).

[29] G. S. Bocharov and A. V. Eletskii, Percolation Conduction of Carbon Nanocomposites, Int. J. Mol. Sci. **21**, 7634 (2020).
[30] H. J. C. Berendsen, in *Computer Simulations in Material Science*, edited by M. Meyer and V. Pontikis (Kluwer, Dordrecht, 1991).
[31] H. J. C. Berendsen, J. P. M. Postma, W. F. van Gunsteren, A. Dinola, and J. R. Haak, J. Chem. Phys. **81**, 3684 (1984).
[32] T. Darden, D. York, and L. Pedersen, J. Chem. Phys. **98**, 10089 (1993).
[33] U. Essmann, L. Perera, M. L. Berkowitz, T. Darden, H. Lee, and L. G. Pedersen, J. Chem. Phys. **103**, 8577 (1995).
[34] S. Datta, *Transport in Mesoscopic Systems* (Cambridge University Press, Cambridge, UK, 1995).
[35] T. Ozaki and H. Kino, Phys. Rev. B **72**, 045121 (2005).
[36] See http://www.openmx-square.org for OpenMX (Open source package for Material eXplorer), a software package for nanoscale material simulations.
[37] I. Morrison, D. M. Bylander, and L. Kleinman, Phys. Rev. B **47**, 6728 (1993).
[38] J. P. Perdew, K. Burke, and M. Ernzerhof, Phys. Rev. Lett. **77**, 3865 (1996).
[39] J. O. Aguilar, J. R. Bautista-Quijano, F. Avilés, Influence of carbon nanotube clustering on the electrical conductivity of polymer composite films, eXPRESS Polymer Letters **4**, 292 (2010).
[40] R. Taherian and A. Kausar, *Electrical Conductivity in Polymer-Based Composites: Experiments, Modelling, and Applications* (William-Andrew, Cambridge, MA, 2019).
[41] W. Xu, X. Su, and Y. Jiao, Phys. Rev. E **94**, 032122 (2016).
[42] T. Schilling, M. A. Miller, and P. Van der Schoot, Europhys. Lett. **111**, 56004 (2015).
[43] M. E. J. Newman and R. M. Ziff, Phys. Rev. E **64**, 016706 (2001).
[44] N. Chiodarelli, S. Masahito, Y. Kashiwagi, Y. Li, K. Arstila, O. Richard, D. J. Cott, M. Heyns, S. De Gendt, G. Groeseneken, and P. M. Vereecken, Nanotechnology **22**, 085302 (2011).
[45] T. W. Ebbesen, H. J. Lezec, H. Hiura, J. W. Bennett, H. F. Ghaemi, and T. Thio, Nature **382**, 54 (1996).
[46] S. Kirkpatrick, Percolation and Conduction, Rev. Mod. Phys. **45**, 574 (1973).
[47] *Polymer Nanotube Nanocomposites: Synthesis, Properties, and Applications*, edited by V. Mittal, 2nd ed. (John Wiley & Sons, Inc., Hoboken, New Jersey, 2014).
[48] G. A. Buxton and A. C. Balazs, Molecular Simulations **30**, 249 (2004).
[49] Y. Zhao, M. Byshkin, Y. Cong, T. Kawakatsu, L. Guadagno, A. De Nicola, N. Yu, G. Milano, and B. Dong, Nanoscale **8**, 15538 (2016).
[50] K. Thorkelsson, J. H. Nelson, A. P. Alivisatos, and T. Xu, End-to-end alignment of nanorods in thin films, Nano Lett. **13**, 4908 (2013).
[51] W. H. Press, S. A. Teukolsky, W. T. Vetterling, and B. P. Flannery, *Numerical Recipes, the Art of Scientific Computing*, 3rd ed. (Cambridge University Press, New York, 2007).
[52] http://ckp.nrcki.ru/.